Isospin-dependent optical potentials in Dirac-Brueckner-Hartree-Fock approach

Jian Rong,[1] Zhong-Yu Ma,[2,1,*] and Nguyen Van Giai[3]
[1]*China Institute of Atomic Energy, Beijing 102413, China*
[2]*China Center of Advanced Science and Technology (World Laboratory), Beijing 100080, China*
[3]*Institut de Physique Nucléaire, IN2P3-CNRS, F-91406 Orsay Cedex, France*
(Received 9 August 2005; published 30 January 2006)

The relativistic microscopic optical potential (RMOP) is studied within the framework of the Dirac-Brueckner-Hartree-Fock (DBHF) approach. A new decomposition of the Dirac structure of nuclear self-energy in the DBHF is extended to asymmetric nuclear matter calculations. A nucleon effective interaction is introduced to reproduce the results of the G matrix. The real part of nucleon self-energy in asymmetric nuclear matter is calculated with the G matrix in the Hartree-Fock approach, while the imaginary part is obtained from the polarization diagram. Nuclear optical potentials in finite nuclei are derived from the self-energies in asymmetric matter through a local-density approximation. The differential cross sections and the analyzing powers in $p + {}^{40}$Ca and $p + {}^{208}$Pb elastic scattering at $E_p \leqslant 200$ MeV are studied with these RMOPs. A satisfactory agreement with the experimental data is found. This is achieved without readjusting phenomenologically the RMOP derived from the DBHF plus polarization diagram.

DOI: 10.1103/PhysRevC.73.014614 PACS number(s): 25.40.−h, 24.10.Jv, 24.10.Cn, 21.65.+f

I. INTRODUCTION

The optical-model potential is an essential tool in nuclear reaction studies. In the past 30 years there has been great interest in the relativistic description of nuclear problems because of the success in reproducing the spin-rotation functions of proton elastic scattering [1] within the relativistic framework. In the relativistic approach, the spin-orbit coupling is directly related to the central (scalar and vector) potentials while in the nonrelativistic approach it is usually adjusted independently. Recently, the relativistic mean-field (RMF) approach has been of great success in describing not only the ground-state properties of stable nuclei, but also those of exotic nuclei. There have also been various applications to investigating nucleon-nucleus scattering. It is well known that the relativistic impulse approximation works successfully in the medium- and high-energy regions [2]. At low energies the medium effects become important; therefore the relativistic optical potential for nucleon-nucleus elastic scattering is usually adopted. By fitting the experimental results, Arnold *et al*. [3] and Hama *et al*. [4] obtained a reasonable global Dirac optical potential with a set of phenomenological parameters for proton-nucleus elastic scattering. It has given reasonable results for elastic scattering off stable nuclei. However, the predictive power of the phenomenological optical potentials is not guaranteed, and therefore extending them to reactions without experimental data, especially to those reactions involving unstable nuclei, remains questionable. It is necessary to investigate the optical potential microscopically in a more fundamental theory. Studies of the relativistic microscopic optical potential (RMOP) in the past few years were based on several models, such as the RMF [5,6], the relativistic Hartree-Fock (RHF) [7], and the Dirac-Brueckner-Hartree-Fock (DBHF) [8–10] approaches. The nucleon self-energies were calculated in symmetric nuclear matter, and the isospin dependence was usually neglected. A reasonable description of the differential cross sections, analyzing powers and spin-rotation functions of proton scattering off stable nuclei has been achieved in an energy range of 50–500 MeV without readjusting parameters [7,9,10].

With the development of experiments on newly constructed radioactive beam facilities, new physical phenomena, such as the neutron and proton halos, have been observed in the past 20 years [11,12]. The density distributions of protons and neutrons in halo and exotic nuclei are very different from normal nuclei. Therefore the isospin dependence of the RMOP becomes important. However, up to now the knowledge about the isospin dependence of the RMOP from experiments is very scarce. The purpose of this paper is to investigate the isospin dependence of the RMOP within the framework of the DBHF approach.

Recently, Schiller and Müther [13] and Ulrych and Müther [14] proposed a new decomposition of the Dirac structure of nucleon self-energies in the DBHF. The DBHF G matrix is separated into a bare nucleon-nucleon (NN) interaction V and a correlation term $\triangle G$. A one-boson exchange potential (OBEP) is usually employed for the bare NN interaction. The coupling constants and meson masses in the OBEP are determined by fitting the phase shifts of the NN scattering and ground-state properties of the deuteron. A projection method is applied to the correlation term $\triangle G$, which is parametrized by four pseudomesons. Therefore the effective NN interaction G in symmetric and asymmetric nuclear matter can be characterized in the RHF approach by the exchanges of those four pseudomesons, in addition to the OBEP. Ma and Liu [15] used this scheme to study the properties of asymmetric nuclear matter and finite nuclei within the RMF framework. Reasonable results were thus achieved.

*Also at the Center of Theoretical Nuclear Physics, National Laboratory of Heavy Ion Accelerator of Lanzhou, Lanzhou 730000, China, and Institute of Theoretical Physics, Chinese Academy of Sciences, Beijing 100080, China.

For scattering problems, the energy dependence of the RMOP is important and it is necessary to work in the RHF approach. This is the method we use in this work.

The optical potential of a nucleon in the nuclear medium is identified with the nucleon self-energy [16]. The same scheme was used to investigate the proton and neutron RMOP in asymmetric nuclear matter [17]. One evaluates the real part of the RMOP in the DBHF approximation by adopting the decomposition of $G = V + \triangle G$. In this work, we extend this approach to investigate the imaginary part of the G matrix, which is calculated as the G-matrix polarization diagram. To avoid ambiguity at low densities and to simplify the calculation of the imaginary part of the RMOP, we adopt an effective phenomenological G matrix that contains four mesons with density-dependent coupling constants. The parameters of the effective interaction are constrained by the real part of the G matrix of Schiller and Müther that reproduces in the RHF approximation the nucleon self-energies of the G matrix in symmetric and asymmetric nuclear matter. The imaginary part of the effective G matrix is predicted from the polarization diagram. The optical potential in finite nuclei is obtained by means of the local-density approximation (LDA), in which the space distribution of the RMOP is directly connected with the density and asymmetry parameters of the nuclear self-energies in the asymmetric nuclear matter. The proton-nucleus scattering with the RMOP is studied, and the isospin dependence of the RMOP is emphasized.

This paper is set up as follows. In Sec. II, we sketch the new decomposition of the Dirac structure of the DBHF G matrix, and we derive the RMOP in nuclear matter. The nucleon effective interaction G_{eff} is introduced in Sec. III. Then, the RMOP in asymmetric nuclear matter is discussed. The RMOP in finite nuclei and a systematic analysis of proton-nucleus scattering with this RMOP are presented in Sec. IV. Finally, a brief summary is given in Sec. V.

II. NUCLEON SELF-ENERGY IN ASYMMETRIC NUCLEAR MATTER

Starting from a bare interaction V fitted to NN scattering phase shifts and deuteron properties, we take the nucleon in-medium short-range correlations into account in the DBHF by summing up all ladder diagrams. We adopt the new decomposition of the DBHF G matrix recently proposed by Schiller and Müther [13]. In this approach, the G matrix can be split into two parts:

$$G = V + \triangle G. \tag{1}$$

Usually, the bare NN interaction V in the DBHF is taken as an OBEP, as in Bonn potentials that contain six mesons with the following spin, parity, and isospin (J^π, T): two scalar mesons, $\sigma(0^+,0)$ and $\delta(0^+,1)$, two vector mesons, $\omega(1^-,0)$ and $\rho(1^-,1)$, and two pseudovector mesons, $\eta(0^-,0)$ and $\pi(0^-,1)$. The correlation term $\triangle G$ is parametrized by four pseudomesons $(\sigma', \delta', \omega', \rho')$. These pseudomesons have infinite masses but finite ratios of coupling constants to the corresponding masses. The couplings have a weak density dependence. Infinite masses depict zero-range interactions. In this way, the ambiguities in the usual projection method can be removed and a satisfactory description of asymmetric nuclear matter and finite nuclei can be achieved [13,14]. Then the nucleon self-energies can be calculated in the RHF with this parametrized G matrix. In this work the bare NN interaction V is taken as Bonn-B and the corresponding parameters for the pseudomesons describing the correlation term $\triangle G$ can be found in Ref. [13].

Because of the translational invariance of homogeneous systems, the DBHF nucleon self-energies in asymmetric nuclear matter have the general form

$$\Sigma^t(k, k_F, \beta) = \Sigma_s^t(k, k_F, \beta) - \gamma_0 \Sigma_0^t(k, k_F, \beta) + \mathbf{f}\gamma \cdot \mathbf{k}\Sigma_v^t(k, k_F, \beta), \tag{2}$$

where t stands for proton or neutron and Σ_s^t, Σ_0^t, and Σ_v^t are the scalar component, timelike, and spacelike parts of the vector component of the self-energy, respectively. They are functions of the nucleon momentum, density, and asymmetry parameter $\beta = (\rho_n - \rho_p)/\rho$, where ρ_n, ρ_p, and ρ are neutron, proton, and matter densities, respectively.

The nucleon self-energy in nuclear matter can be calculated in RHF with the V and $\triangle G$ of Eq. (1). In asymmetric nuclear matter, the Fermi momenta of protons and neutrons are different. Therefore proton and neutrons have to be distinguished. Here, we adopt simplified notation in which the proton and neutron indices are omitted unless they are necessary. The nucleon self-energy is expressed as

$$\Sigma(k, k_F, \beta) = \sum_\alpha \int \frac{d^4q}{(2\pi)^4} \left\{ \Gamma_\alpha^a \Delta_\alpha^{ab}(0) \mathrm{Tr}\left[i\Gamma_\alpha^b \mathcal{G}(q) \right] - i\Gamma_\alpha^a \Delta_\alpha^{ab}(q) \Gamma_\alpha^b \mathcal{G}(k-q) \right\}, \tag{3}$$

where the first and second terms correspond to direct (Hartree) and exchange (Fock) terms, respectively. The index α refers to mesons, a and b are isospin components, $\mathcal{G}$ is the single-particle Green's function, and Δ_α^{ab} are meson propagators. The vertices Γ_α^a correspond to ig for scalar mesons, $-g\gamma^\mu$ for vector mesons, and $-\frac{f}{m}\gamma^5\gamma^\mu q_\mu$ for pseudovector mesons. They are multiplied by the isospin operator τ_a for isovector mesons. The nucleon propagator $\mathcal{G}$ can be divided into two parts, the Feynman part $\mathcal{G}_F$ and the density-dependent part $\mathcal{G}_D$. The $\mathcal{G}_F$ part produces a divergent vacuum tadpole contribution to the nucleon self-energy. It is neglected in DBHF calculations. The density-dependent part $\mathcal{G}_D$ is expressed as

$$\mathcal{G}_D(k) = T_t[\gamma^\mu k_\mu^* + M^*(k)] \frac{i\pi}{E^*} \delta(k_0 - \varepsilon)\theta(k_F - |\mathbf{k}|), \tag{4}$$

where

$$\begin{aligned} M^*(k) &= M + \Sigma_s(k), \\ E^*(k) &= \sqrt{\mathbf{k}^{*2} + M^{*2}(k)}, \\ k_\mu^*(k) &= \{k_0 + \Sigma_0(k), \mathbf{k}[1 + \Sigma_v(k)]\}, \end{aligned} \tag{5}$$

and T_t is the isospin operator:

$$T_t = \tfrac{1}{2}(1 \pm \tau_3), \tag{6}$$

where the plus (minus) sign corresponds to protons (neutrons).

Let us first work out the isospin part of the self-energies. In the direct terms, the contributions of isoscalar and isovector

mesons are, respectively,

$$\begin{aligned} I\,\mathrm{Tr}(T_i I) &= I, \\ \tau_a\,\mathrm{Tr}(T_i \tau_b)\delta_{ab} &= \pm\tau_3. \end{aligned} \tag{7}$$

In the exchange terms the corresponding contributions are

$$\begin{aligned} I T_i I &= \tfrac{1}{2}(1 \pm \tau_3), \\ \tau_a T_i \tau_b \delta_{ab} &= \tfrac{1}{2}(3 \mp \tau_3). \end{aligned} \tag{8}$$

In Eqs. (7) and (8), the upper (lower) sign corresponds to protons (neutrons).

The momentum of a nucleon of energy $\varepsilon = E + M$ in the nuclear medium can be calculated by iteration:

$$\begin{aligned} \varepsilon &= [\varepsilon^* - \Sigma_0(k)]_{k_0=\varepsilon} \\ &= \sqrt{\mathbf{k}^2[1+\Sigma_v(k)]^2 + [M+\Sigma_s(k)]} - \Sigma_0(k). \end{aligned} \tag{9}$$

Therefore the momentum dependence of the nucleon self-energy at a given density is related to the energy dependence of the RMOP.

It has been shown [17] that the direct term in Eq. (3) is a dominant part of the nucleon self-energy. This part is momentum independent and therefore energy independent. The energy and momentum dependences come only from the exchange part. Furthermore, the contribution of the correlation term ΔG to the nucleon self-energies characterized by pseudomeson exchanges is also energy independent because of the zero-range nature of these pseudomesons.

The imaginary part of the optical potential is obtained by the G-matrix polarization diagram, which is shown in Fig. 1. The exchange contribution is ignored here; it is discussed in more detail in Ref. [18]. The contribution of the G-matrix polarization diagram to the nucleon self-energy can be calculated as follows:

$$\begin{aligned} \Sigma_{\mathrm{pol}}(k) = \sum_{\alpha\beta} \int \frac{d^4q}{(2\pi)^4} \Bigg(& \Gamma^a_\alpha \Delta^{ab}_\alpha(q) \int \frac{d^4p}{(2\pi)^4} \\ & \times \mathrm{Tr}\left\{\Gamma^b_\alpha [i\mathcal{G}(p)] \Gamma^c_\beta [i\mathcal{G}(p+q)]\right\} \\ & \times \Delta^{cd}_\beta(q) [i\mathcal{G}(k-q)] \Gamma^d_\beta \Bigg). \end{aligned} \tag{10}$$

By Wick rotation, the imaginary part W of Σ_{pol} can be derived and its Lorentz components can be projected by taking traces

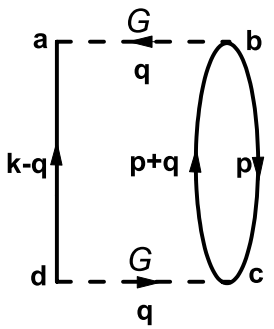

FIG. 1. The G-matrix polarization diagram.

as follows:

$$\begin{aligned} W_s(k) &= \frac{1}{4}\mathrm{Tr}\, W(k), \\ W_0(k) &= \frac{1}{4}\mathrm{Tr}\,\gamma^0 W(k), \\ W_v(k) &= \frac{1}{4k^2}\mathrm{Tr}\,\vec{k}\cdot\vec{\gamma} W(k). \end{aligned} \tag{11}$$

The isospin part in the polarization diagram is more complicated. There are two particles (i, j) and one hole (k) in the intermediate states and exchanging two effective mesons. One can distinguish three cases: (a) exchanging two isoscalar mesons, (b) one isoscalar and one isovector meson, (c) two isovector mesons. Their contributions to the isospin part are as follows, respectively:

$$I T_i I\,\mathrm{Tr}(T_k I T_j I) = T_i, \tag{12a}$$

$$\begin{aligned} &\tau_a T_i I\,\mathrm{Tr}(T_k \tau_a T_j I) \\ &\quad = \begin{cases} T_i, \ i, \text{ and } j \text{ have same isospins} \\ -T_i, \ i \text{ and } j \text{ have opposite isospins} \end{cases}, \end{aligned} \tag{12b}$$

$$\begin{aligned} &\tau_a T_i \tau_b\,\mathrm{Tr}(T_k \tau_a T_j \tau_b) \\ &\quad = \begin{cases} \tfrac{1}{2}(3 \mp \tau_3), \ j \text{ and } k \text{ have same isospins} \\ 2, \ j \text{ and } k \text{ have opposite isospins} \end{cases}. \end{aligned} \tag{12c}$$

III. NUCLEON EFFECTIVE INTERACTION

In principle the imaginary part of Eq. (10) could be calculated with the G matrix. It was found earlier that the pion exchange in the bare NN interaction V makes a large contribution to the imaginary part of the polarization diagram [7]. The reason for this unphysically large contribution may be due to high-order correlations in the pion exchange. We also find that this large contribution to the imaginary part of the polarization diagram cannot be eliminated by the correlation term ΔG. To avoid this problem we introduce an effective nucleon interaction G_{eff} that reproduces the real part of nucleon self-energies and properties of the symmetric and asymmetric nuclear matter as given by $G = V + \Delta G$.

The effective nucleon interaction consists of four scalar and vector pseudomesons with isoscalar and isovector characters, corresponding to σ, ω, δ, and ρ mesons. The masses of these effective mesons are fixed and the coupling constants are adjusted in the RHF to reproduce the DBHF results in the scheme of $G = V + \Delta G$, namely, the neutron and proton self-energies as well as the binding energy at each density in the symmetric and asymmetric nuclear matter. To extend to low densities, an extrapolation is employed. The coupling constants are density dependent and are given by the following expressions [19,20]:

$$\begin{aligned} g_i(\rho) &= g_i(\rho_0) f_i(x), \\ f_i(x) &= a_i \frac{1 + b_i(x+d_i)^2}{1 + c_i(x+d_i)^2}. \end{aligned} \tag{13}$$

where $x = \rho/\rho_0$, and $i = (\sigma, \omega, \delta, \rho)$, ρ and ρ_0 are the matter density and the saturation density of nuclear matter,

TABLE I. Parameters of the nucleon effective interaction $G_{\rm eff}$.

Parameter	σ	ω	δ	ρ
Mass (MeV)	550	782.6	938	769
$g_i(\rho_0)$	5.851	7.329	0.860	0.514
a_i	1.8059	1.8197	0.9273	11.473
b_i	0.1046	0.1019	0.4620	−0.2394
c_i	0.4123	0.4128	0.4084	0.5415
d_i	0.8992	0.8985	0.9035	0.7846

respectively, and a_i, b_i, c_i, d_i are parameters determined by the fitting procedure with the following constraining conditions:

$$f_i(1) = 1, \quad \left.\frac{d^2 f_i(x)}{dx^2}\right|_{x=0} = 0. \tag{14}$$

These constraints ensure that the coupling constants at the saturation density are unchanged and have reasonable behaviors near zero density. The parameters are listed in Table I, and the density dependence of the coupling constants is plotted in Fig. 2. Curves are depicted by Eqs. (13), and symbols represent the fits of DBHF results. The energies per nucleon at various values of the asymmetry parameter are shown in Fig. 3, in which the curves are calculated in RHF with $G_{\rm eff}$ and symbols are obtained in the DBHF.

With this nucleon effective interaction we calculate the nucleon self-energies at $E > 0$:

$$\Sigma^t = \widetilde{U}^t + i W^t, \tag{15}$$

where $\widetilde{U}^t$ and W^t are calculated in Eqs. (3) and (10), respectively.

The optical potential of a nucleon in the nuclear medium is its self-energy [16]. For finite nuclei it is obtained by means

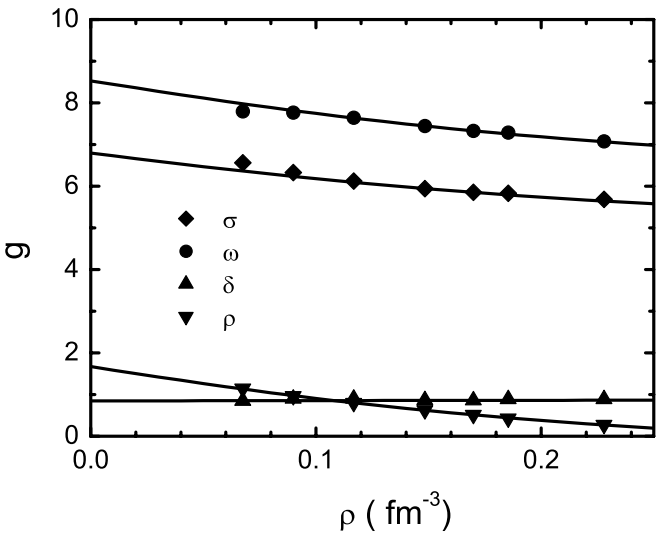

FIG. 2. The density dependence of the coupling constants in $G_{\rm eff}$. The curves correspond to Eqs. (13), and the symbols show the values needed to reproduce the DBHF results with $G = V + \Delta G$.

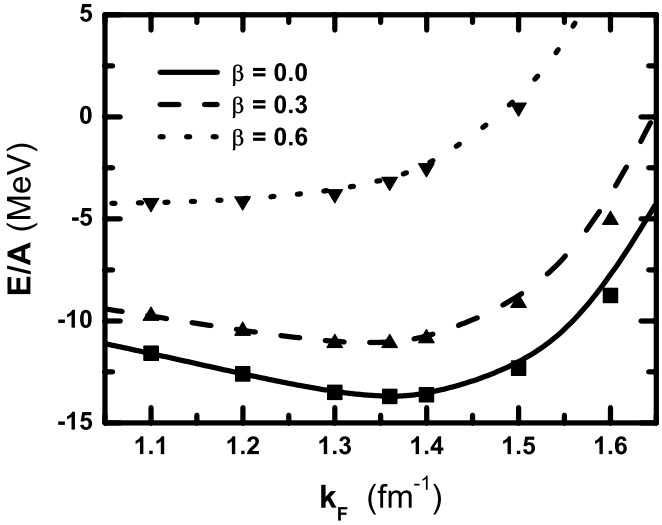

FIG. 3. Energy per nucleon as a function of the nucleon density in symmetric and asymmetric nuclear matter. Curves are RHF results with $G_{\rm eff}$; symbols represent DBHF results corresponding to $G = V + \Delta G$.

of the LDA, in which the space dependence of the RMOP is directly connected with the density and asymmetry parameter in asymmetric nuclear matter:

$$\Sigma_{\rm LDA}(r, E) = \Sigma_{\rm NM}[k, \rho(r), \beta], \tag{16}$$

where $\Sigma_{\rm LDA}$ is the optical potential for a finite nucleus with incident nucleon energy E, and $\Sigma_{\rm NM}$ is the optical potential in nuclear matter at density ρ and asymmetry parameter β.

The Dirac equation of a nucleon with incident energy E in the nuclear medium has the form

$$\left[\vec{\alpha}\cdot\vec{p} + \gamma_0\left(M + U_s^t\right) + U_0^t\right]\psi^t(\vec{r}) = \varepsilon\psi^t(\vec{r}), \tag{17}$$

where

$$U_s^t = \frac{\Sigma_s^t - \Sigma_v^t M}{1 + \Sigma_v^t}, \qquad U_0^t = \frac{-\Sigma_0^t + E\Sigma_v^t}{1 + \Sigma_v^t}, \tag{18}$$

with $\varepsilon = E + M$, and U_s^t and U_0^t are the scalar and vector potential, respectively.

The scalar and vector potentials in asymmetric nuclear matter at $k_F = 1.36$ fm^{-1} are calculated with the nucleon effective interaction. The real and imaginary parts of the scalar potential U_s and vector potential U_0 of protons and neutrons as functions of the asymmetry parameter β are shown in Figs. 4 and 5. For symmetric nuclear matter, it is found that Re U_s is about −330 MeV at the Fermi surface and −280 MeV at $E = 400$ MeV. The scalar mass $M^*/M = 1 + {\rm Re}\, U_s/M$ varies from 0.65 at the Fermi surface to 0.70 at $E = 400$ MeV. The vector potential Re U_0 decreases from 260 to 200 MeV. These results are consistent with those obtained in Ref. [8]. It can be seen in Fig. 4 that, at low energies, the real parts of both scalar and vector potentials for protons become weaker as β increases. Interestingly, their energy dependence in asymmetric nuclear matter becomes weaker than in symmetric nuclear matter. Therefore, at a certain energy, the strengths of

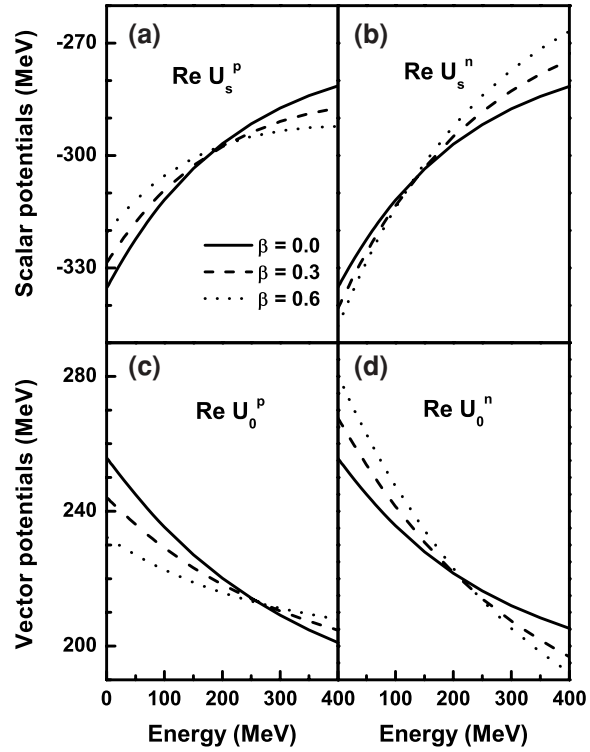

FIG. 4. Real parts of scalar and vector potentials at $k_F = 1.36\,\mathrm{fm}^{-1}$ for various values of β: (a) proton scalar potential Re U_s^p; (b) neutron scalar potential Re U_s^n; (c) and (d) are the corresponding quantities for the vector potential.

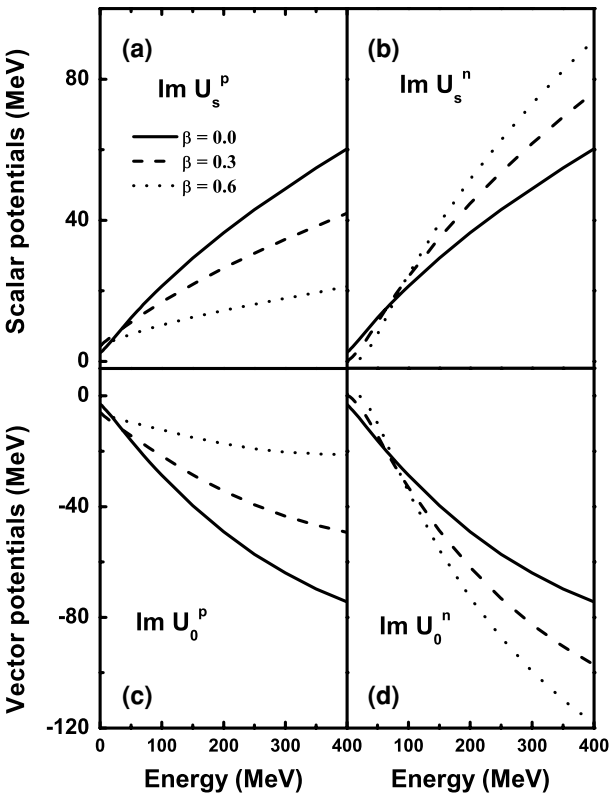

FIG. 5. Same as Fig. 4, but for imaginary parts of the scalar and vector potentials.

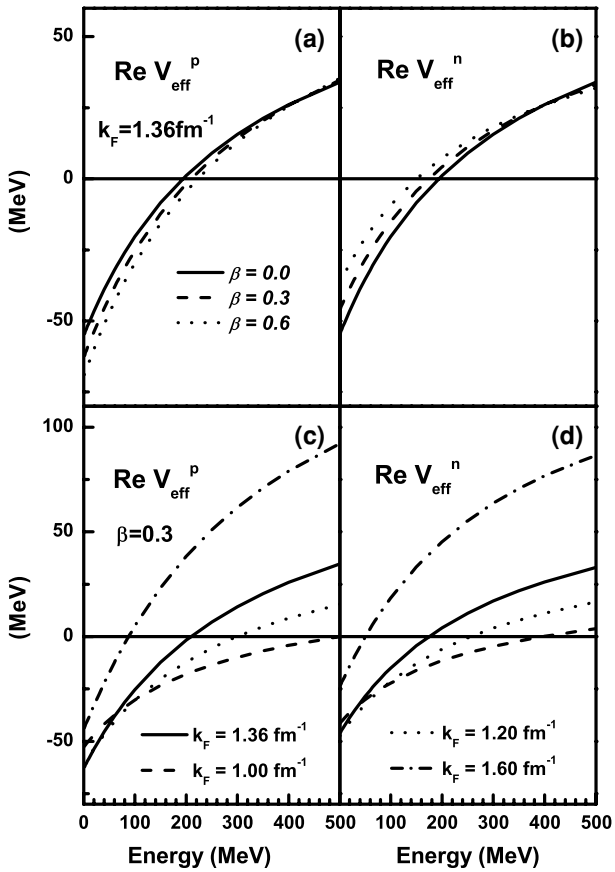

FIG. 6. The depths of the real part of Schrödinger equivalent potentials as functions of incident energy: (a) protons, at fixed k_F and various β; (b) same as (a), but for neutrons; (c) protons, at fixed β and various k_F; (d) same as (c), but for neutrons.

Re U_s^p and Re U_0^p become stronger than those in symmetric nuclear matter. The situation for neutrons is the opposite. In asymmetric matter the magnitudes of the scalar and vector potentials for neutrons at low energies are larger than in symmetric matter, and their energy dependence becomes stronger as β increases. There are crossing points, as one can see in Fig. 4.

On the other hand, imaginary parts of both scalar and vector potentials become stronger as the energy increases, although their strengths are somewhat smaller than those of the real parts at low energies, as shown in Fig. 6. The energy dependence of neutron potentials becomes stronger in neutron-rich matter, while that of proton potentials becomes weaker. These properties are consistent with the findings of phenomenological potentials.

When the lower component of the Dirac spinor in Eq. (17) is eliminated, a Schrödinger-type equation is obtained for the upper component:

$$\left[-\frac{\nabla^2}{2E} + V^t_{\mathrm{eff}}(r) + V^t_{\mathrm{s.o.}}(r)\vec{\sigma}\cdot\vec{\mathbf{L}} + V^t_{\mathrm{Darwin}}(r)\right]\varphi(\mathbf{r}) = \frac{\varepsilon^2 - M^2}{2E}\varphi(\mathbf{r}), \tag{19}$$

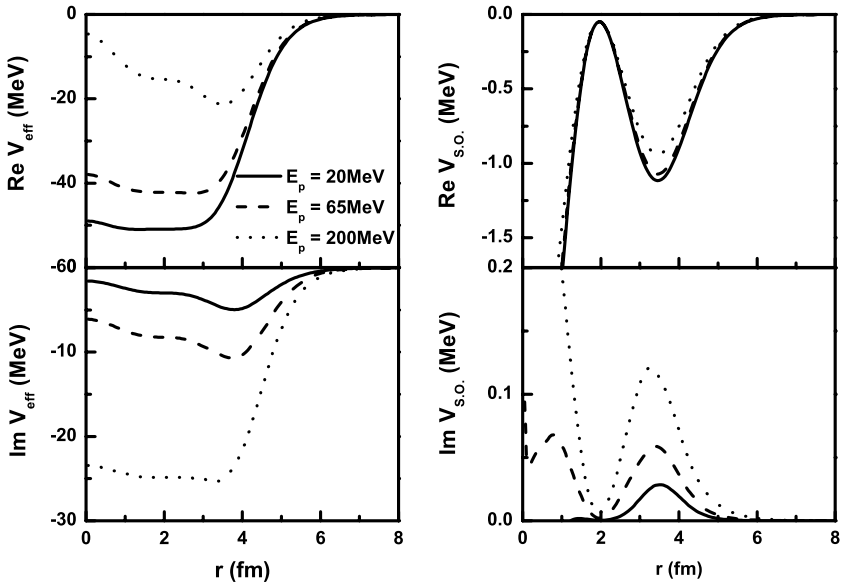

FIG. 7. The shapes of Schrödinger equivalent potentials in $p + {}^{40}$Ca at 20 MeV (solid curves), 65 MeV (dashed curves), and 200 MeV (dotted curves).

where $V^t_{\rm eff}$, $V^t_{\rm s.o.}$ and $V^t_{\rm Darwin}$ are the central, spin-orbit, and Darwin potentials, respectively:

$$V^t_{\rm eff} = \frac{M}{E}U^t_s + U^t_0 + \frac{1}{2E}\left[U^{t2}_s - \left(U^t_0 - V_c\right)^2\right],$$
$$V^t_{\rm s.o.} = -\frac{1}{2ErD^t(r)}\frac{dD^t(r)}{dr}, \qquad (20)$$
$$V^t_{\rm Darwin} = \frac{3}{8ED^t(r)}\left[\frac{dD^t(r)}{dr}\right]^2 - \frac{1}{2ErD^t}\frac{dD^t}{dr} - \frac{1}{4ED^t(r)}\frac{d^2D^t(r)}{d^2r},$$

where $D^t(r) = M + \varepsilon + U^t_s(r) - U^t_0(r) - V_c(r)$ and V_c is the Coulomb potential (only for protons).

One can see from Eqs. (20) that the central potential $V_{\rm eff}$ is obtained by a large cancellation between the scalar and vector potential, which is roughly equal to $U_s + U_0$ at low energy and $\frac{1}{2}U_s + U_0$ at energies around 1 GeV. Therefore its sign changes from negative to positive with the increase of incident energies. The energy dependence of the Schrödinger equivalent central potentials Re $V^p_{\rm eff}$ and Re $V^n_{\rm eff}$ at $k_F = 1.36$ fm^{-1} for various values of β are shown in Figs. 6(a) and 6(b), respectively. They are attractive at low energies and become repulsive around 100–300 MeV, depending on β. The strength of the proton central potential Re $V^p_{\rm eff}$ and its energy dependence become stronger as β increases at low energies, whereas the situation for the neutron potential Re $V^n_{\rm eff}$ is opposite.

The density dependence of proton and neutron central potentials, Re $V^p_{\rm eff}$ and Re $V^n_{\rm eff}$ in asymmetric nuclear matter with $\beta = 0.3$ is shown in Figs. 6(c) and 6(d), respectively. In general, the neutron potential is weaker than that of the proton. The central potentials at densities smaller than normal density ρ_0 become more attractive around 100–300 MeV, where a "wine-bottle bottom" potential for finite nuclei will appear [7].

IV. ELASTIC PROTON-NUCLEUS SCATTERING

To analyze the proton-nucleus scattering reactions, the density distributions of finite nuclei should be first determined. In this work, the density distribution of finite nuclei are calculated in the RMF theory with the parameter set NL3 [21] because it well describes finite nuclei properties.

We investigate elastic proton scattering off spherical nuclei, such as $p + {}^{40}$Ca and $p + {}^{208}$Pb. The shapes of Schrödinger equivalent potentials at various incident energies are shown in Fig. 7. The depth of the real part of the central potential decreases as the energy increases. At intermediate energies around $E_p \simeq 150$ MeV, an attractive pocket at the nuclear surface is found. The so-called wine-bottle bottom shape appears, which comes from the delicate balance between U_s and U_0. Unlike the strength of the real part, the strength of the imaginary part of the central potential increases as the energy increases. The surface-peaked shape at low energies becomes more of a volume type at higher energies. The important feature of the RMOP is that the spin-orbit potential arises naturally from the coherent sum of the contributions

TABLE II. $\sigma(\theta)$ and $A_y(\theta)$ databases for proton elastic scattering.

Target	Ref.	Energy (MeV)	Ref.	Energy (MeV)
^{40}Ca	[22]	14.5,18.6,19.6,21	[30]	65
	[23]	16	[31]	75,152
	[24]	21,48,49	[32]	80.2,160,181
	[25,26]	26.3,30.3	[33]	135.1
	[27]	35.5,45.5	[34]	156
	[28]	40	[35]	200,201
	[29]	61.4		
^{208}Pb	[36]	11,12,13	[29]	62.4
	[23]	16	[30]	65
	[37]	21,24.1,35,45, 47.3,155,185	[33]	79.9,100.4, 121.2,182.4
	[25]	26.3	[32]	79.9,98,185
	[26,38]	30.3	[34]	156
	[28]	40	[40]	160
	[39]	49.4	[41]	201

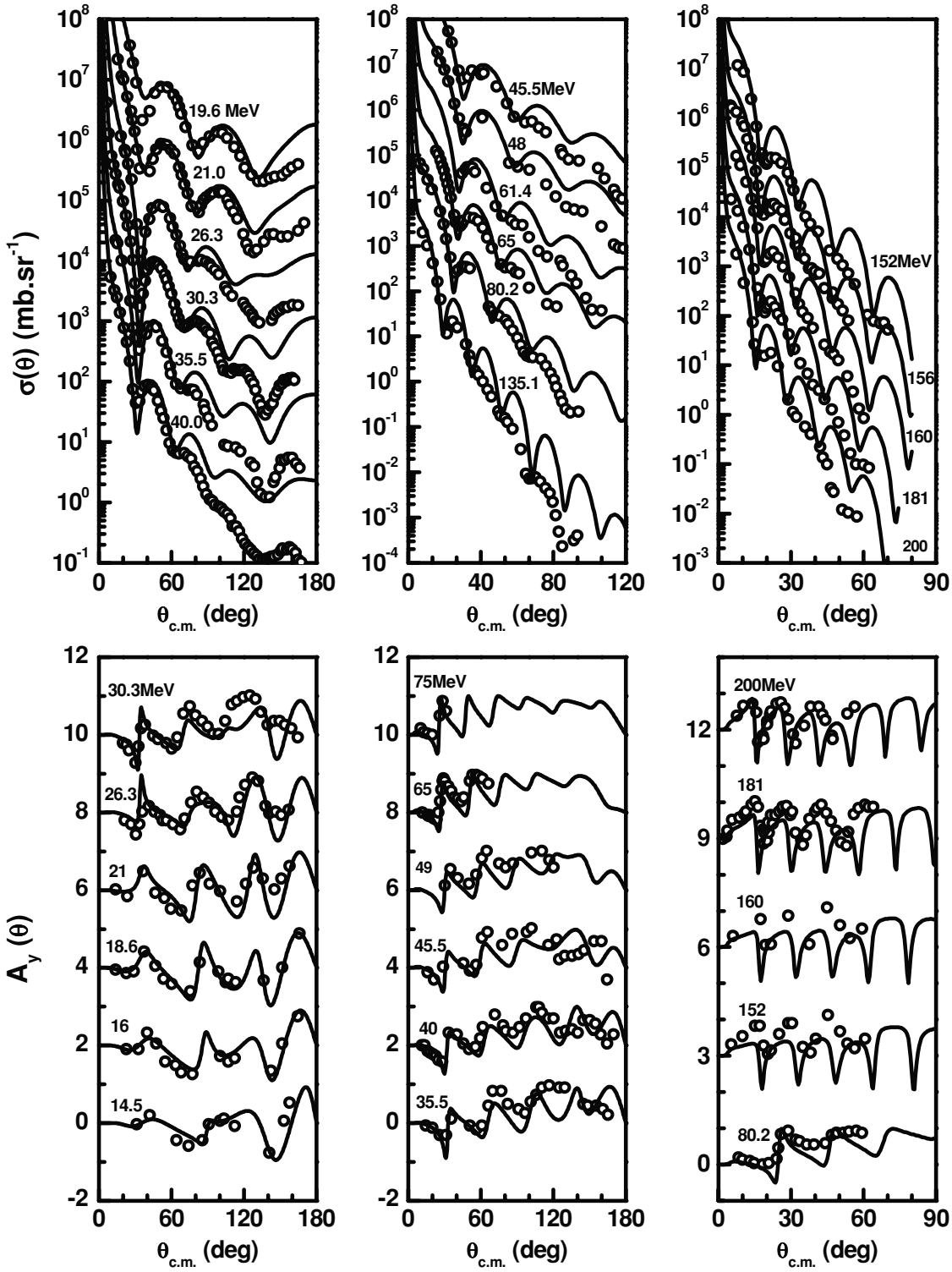

FIG. 8. Elastic scattering differential cross sections and analyzing powers in $p + {}^{40}$Ca at $E_p < 200$ MeV. Note that the differential cross sections are offset by powers of 10 and the analyzing powers are shifted by increments of 2 (for $E_p < 80$ MeV) and 3 (for $E_p > 80$ MeV).

from the scalar and vector potentials. The real part of the spin-orbit potential is attractive, with its strength decreasing as the energy increases, whereas its imaginary part is mostly positive and increasing with the energy. These features of the microscopic optical potentials are very similar to what is found in the phenomenological optical potentials. We calculate the differential cross sections, analyzing powers and spin-rotation functions of $p + {}^{40}$Ca and $p + {}^{208}$Pb at various values of $E_p < 200$ MeV and compare with the experimental data. The references of the experimental data are listed in Table II.

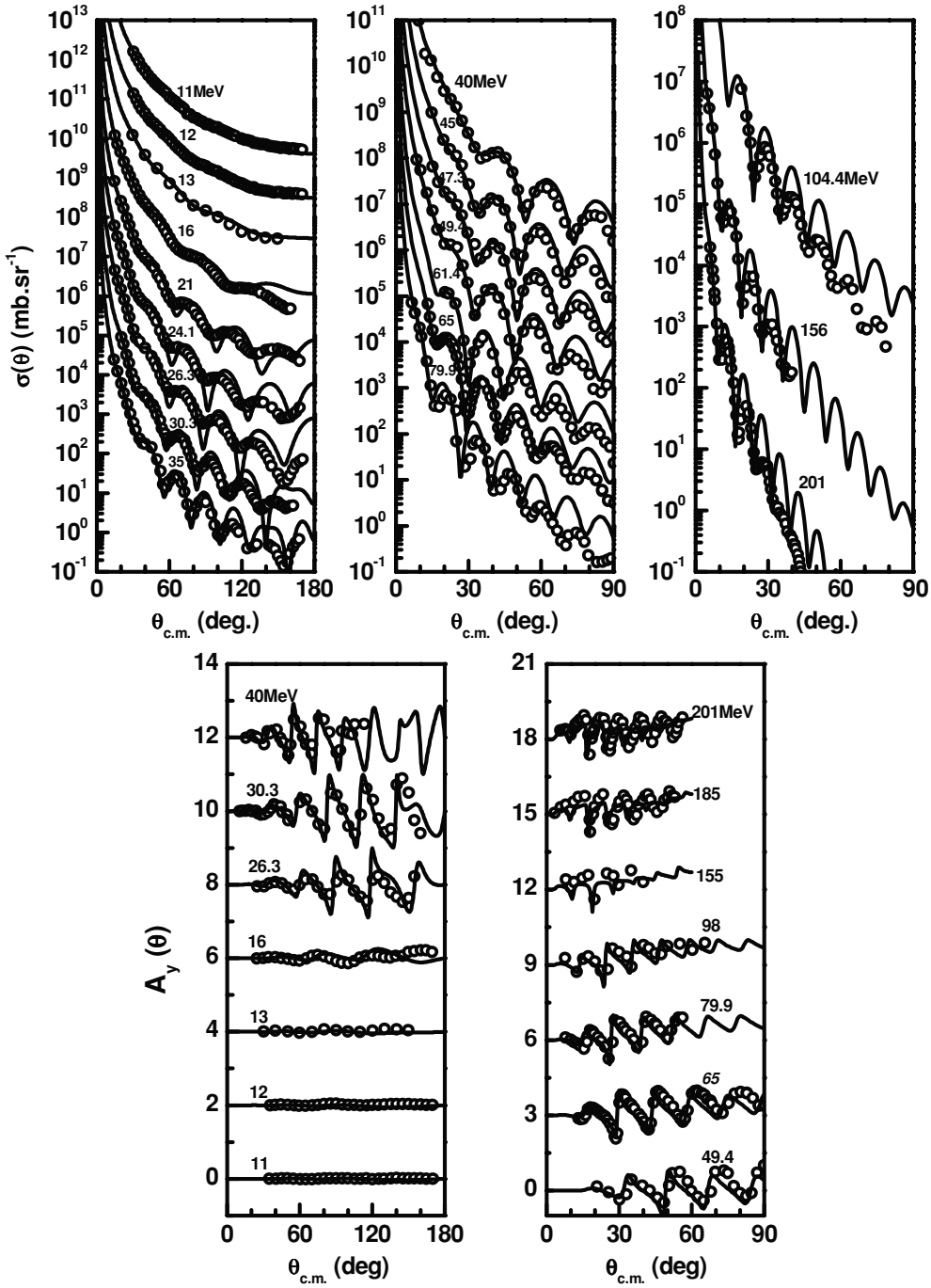

FIG. 9. Elastic scattering differential cross sections and analyzing powers in $p + {}^{208}$Pb at $E_p < 200$ MeV. Note that the differential cross sections are offset by powers of 10 (for $E_p < 100$ MeV) and 100 (for $E_p > 100$ MeV), while the analyzing powers are shifted by increments of 2 (for $E_p < 50$ MeV) and 3 (for $E_p > 50$ MeV), respectively.

In Figs. 8 and 9, we show the comparison of the theoretical results (solid curves) with the experimental data of $\sigma(\theta)$ and $A_y(\theta)$ for $p + {}^{40}$Ca and $p + {}^{208}$Pb, respectively. The spin-rotation functions are plotted in Fig. 10. It is found that the calculated cross sections as well as spin observables are in rather good agreement with the experimental data at low energies. As the energy increases, the theoretical differential cross sections are overestimated at large angles in comparison with the experimental data, but they keep the same diffraction patterns. It seems that the Schrödinger equivalent potentials obtained in our calculations are a little too strong. It should be stressed that the RMOP is calculated microscopically with the nucleon effective interaction without readjusting parameters to fit the scattering data. The nucleon effective interaction is directly extracted from the DBHF G matrix. Since our calculations are parameter free in the scattering analysis, the quality of agreement with the experimental data is remarkable.

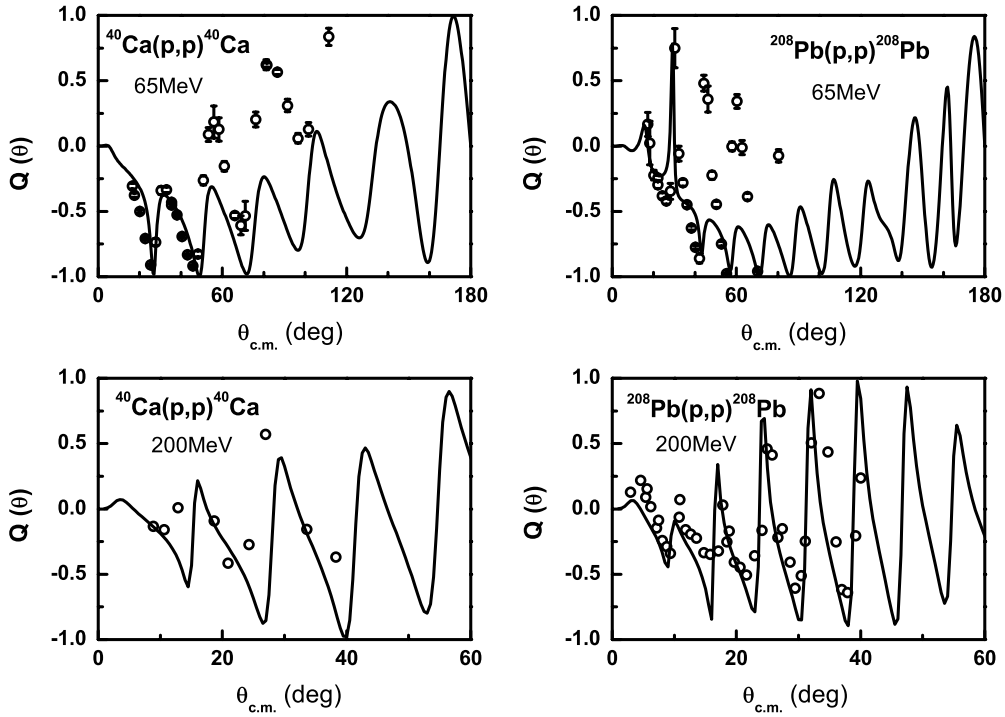

FIG. 10. The spin-rotation functions in $p + {}^{40}$Ca and $p + {}^{208}$Pb at $E_p = 65$ MeV and $E_p = 200$ MeV.

In the phenomenological optical potential, the Lane potential was introduced to depict the difference between proton and neutron optical potentials [42]. The optical potential is divided into isoscalar and isovector components:

$$V = V_0 + \frac{\mathbf{t} \cdot \mathbf{T}}{A} V_1, \tag{21}$$

where A is the nuclear mass, and $\mathbf{t}$ and $\mathbf{T}$ are isospin operators of the incident particle and target, respectively. The Lane potential V_1 is usually parametrized with a Woods-Saxon shape. We calculate the RMOP of protons and neutrons in ^{208}Pb at $E = 65$ MeV and extract the corresponding Lane potential shown in Fig. 11. The phenomenological Lane potential is taken as $V_1 = 50$ MeV, with Woods-Saxon parameters $r_0 = 1.17$ fm and $a = 0.75$ fm. It is shown for comparison in Fig. 11. The agreement indicates that the RMOP obtained from the G matrix can reasonably describe the isospin dependence of the optical potential.

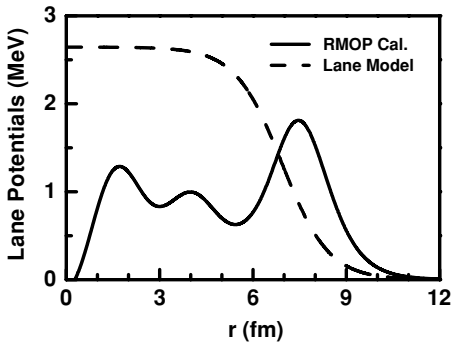

FIG. 11. The Lane potential of $p + {}^{208}$Pb at 65 MeV. The solid curve is calculated in the RMOP, and the dashed curve is a phenomenological one.

V. SUMMARY

In this work, we investigated the relativistic microscopic optical potential and its isospin dependence in asymmetric nuclear matter within the framework of the DBHF approach. The new decomposition of the Dirac structure of the G matrix, $G = V + \triangle G$, is adopted, where V is the Bonn-B potential and $\triangle G$ is characterized by four pseudomesons with infinite masses and finite ratios of the coupling constants to the masses. The nucleon self-energy is calculated with this G matrix in the RHF approach. The imaginary part of the nucleon self-energy with $E > 0$ is obtained by the G-matrix polarization diagram. The self-energy of unbound nucleon in nuclear matter is investigated. To simplify the calculation and avoid the contribution of higher-order correlations from the pion exchange in the imaginary part of the nucleon self-energy we introduce a nucleon effective interaction. The nucleon effective interaction could reproduce the nucleon self-energy as well as nuclear matter properties. The optical potential of a nucleon in the nuclear medium is identified with the nucleon self-energy. The energy and asymmetric parameter dependences of the relativistic optical potentials for proton and neutron are discussed. The resulting Schrödinger equivalent potentials have reasonable behaviors of the energy dependence. The asymmetric parameter dependence of the RMOP and Schrödinger equivalent potentials is emphasized.

The nucleon-nucleus optical potentials in finite nuclei are related to the self-energy in nuclear matter by means of the LDA, in which the target density is determined by the

RMF with the parameters NL3. With the optical potentials determined, we calculated differential cross sections and spin observables of $p + {}^{40}$Ca and $p + {}^{208}$Pb at $E_p < 200$ MeV. The agreement with the experimental data is reasonable. It should be emphasized that the RMOP obtained from the DBHF G matrix without free parameters could well describe proton elastic scattering. It is quite encouraging that the microscopic method could well describe the proton scattering from various target nuclei in a quite large energy region, $E < 200$ MeV. The further application of this RMOP to exotic nuclei is in progress.

ACKNOWLEDGMENTS

This work is supported by the National Natural Science Foundation of China under Grant Nos. 10235020, 10275094, 10535010 and 10475116, and Major State Basic Research Development Programme in China under Contract Nos. G1999022603 and G2000077400, and is also partially supported by the European Community project Asia-Europe Link in Nuclear Physics and Astrophysics, CN/ASIA-LINK/008(94791). The support of the CNRS (France)–NSFC (China) collaboration agreement is acknowledged.

[1] B. C. Clark, R. L. Mercer, and P. Schwandt, Phys. Lett. **B122**, 211 (1983).
[2] J. A. McNeil, J. R. Shepard, and S. J. Wallace, Phys. Rev. Lett. **50**, 1439 (1983).
[3] L. G. Arnold, B. C. Clark, R. L. Mercer, and P. Schwandt, Phys. Rev. C **23**, 1949 (1981).
[4] S. Hama, B. C. Clark, E. D. Cooper, H. S. Sherif, and R. L. Mercer, Phys. Rev. C **41**, 2737 (1990).
[5] C. J. Horowitz and B. D. Serot, Nucl. Phys. **A399**, 529 (1983).
[6] C. J. Horowitz, Nucl. Phys. **A412**, 228 (1984).
[7] Ma Zhong-yu, Zhu Ping, Gu Ying-qi *et al*., Nucl. Phys. **A490**, 619 (1988).
[8] Ma Zhong-yu and Chen Bao-qiu, J. Phys. G **18**, 1543 (1992).
[9] G. Q. Li, R. Machleidt, R. Fritz, H. Müther, and Y. Z. Zhuo, Phys. Rev. C **48**, 2443 (1993).
[10] B. Q. Chen and A. D. Mackellar, Phys. Rev. C **52**, 878 (1995).
[11] T. Tanihata *et al*., Phys. Lett. **B160**, 380 (1985).
[12] R. F. Casten and B. M. Sherrill, Prog. Part. Nucl. Phys. **45**, s171 (2000).
[13] E. Schiller and H. Müther, Eur. Phys. J. A **11**, 15 (2001).
[14] S. Ulrych and H. Müther, Phys. Rev. C **56**, 1788 (1997).
[15] Z. Y. Ma and L. Liu, Phys. Rev. C **66**, 024321 (2002).
[16] J. S. Bell and E. J. Squires, Phys. Rev. Lett. **3**, 96 (1959).
[17] J. Rong and Z. Y. Ma, Science in China G: Physics Astronomy **33**, 481 (2003).
[18] Y. L. Han, Q. B. Shen, Y. Z. Zhuo, and T. M. Geng, High Energy Phys. and Nucl. Phys. **17**, 751 (1993) (in chinese).
[19] S. Typel and H. Wolter, Nucl. Phys. **A656**, 331 (1999).
[20] W. Long, J. Meng, N. Van Giai, and S. G. Zhou, Phys. Rev. C **69**, 034319 (2004).
[21] G. A. Lalazissis, J. König, and P. Ring, Phys. Rev. C **55**, 540 (1997).
[22] E. T. Boschitz, R. W. Bercaw, and J. S. Vincent, Phys. Lett. **13**, 322 (1964).
[23] R. L. Varner *et al*., Phys. Rep. **201**, 57 (1991).
[24] K. H. Bray *et al*., Nucl. Phys. **A167**, 57 (1971).
[25] D. L. Watson *et al*., Nucl. Phys. **A92**, 193 (1967).
[26] B. W. Ridley and J. F. Turner, Nucl. Phys. **A58**, 497 (1964).
[27] E. E. Gross *et al*., Nucl. Phys. **A102**, 673 (1967).
[28] L. N. Blumberg *et al*., Phys. Rev. **147**, 812 (1966).
[29] C. B. Fulmer *et al*., Phys. Rev. **181**, 1565 (1969).
[30] H. Sakaguchi, M. Nakamura, K. Hatanaka, A. Goto, T. Noro, F. Ohtani, H. Sakamoto, H. Ogawa, and S. Kobayashi, Phys. Rev. C **26**, 944 (1982).
[31] C. Rolland *et al*., Nucl. Phys. **80**, 625 (1966).
[32] P. Schwandt, H. O. Meyer, W. W. Jacobs, A. D. Bacher, S. E. Vigdor, M. D. Kaitchuck, and T. R. Donoghue, Phys. Rev. C **26**, 55 (1982).
[33] A. Nadasen, P. Schwandt, P. P. Singh, W. W. Jacobs, A. D. Bacher, P. T. Debevec, M. D. Kaitchuck, and J. T. Meek, Phys. Rev. C **23**, 1023 (1981).
[34] V. Comparat *et al*., Nucl. Phys. **A221**, 403 (1974).
[35] H. Seifert *et al*., Phys. Rev. C **47**, 1615 (1993), and references therein.
[36] W. Kretschmer *et al*., Phys. Lett. **B87**, 343 (1975).
[37] W. T. H. van Oers *et al*., Phys. Rev. C **10**, 307 (1974).
[38] G. W. Greenless *et al*., Phys. Rev. C **2**, 1063 (1970).
[39] G. S. Mandi, D. T. Jones, and D. Jacques, Nucl. Phys. **A165**, 384 (1971).
[40] P. G. Roos and N. S. Wall, Phys. Rev. **140**, B1237 (1965).
[41] N. Ottenstein, S. J. Wallace, and J. A. Tjon, Phys. Rev. C **38**, 2272 (1988), and references therein.
[42] A. M. Lane, Phys. Rev. Lett. **8**, 171 (1962); Nucl. Phys. **35**, 676 (1962) .